Langmuir

ARTICLE

pubs.acs.org/Langmuir

Microscopic Study of Hydroxyapatite Dissolution As Affected by Fluoride Ions

Ki-Young Kwon,[†,‡] Eddie Wang,[†] Michel Nofal,[†] and Seung-Wuk Lee[*,†]

[†]Department of Bioengineering, University of California, Berkeley, and Physical Biosciences Division, Lawrence Berkeley National Laboratory, Berkeley, California 94720, United States

[‡]Department of Chemistry and RINS, Gyeongsang National University, Jinju 660-701, South Korea

Supporting Information

ABSTRACT: Fluoride ions play a critical role in preventing tooth decay. We investigated the microscopic effects of fluoride ions on hydroxyapatite (100) surface dissolution using in situ atomic force microscopy. In the presence of 10 mM NaF, individual surface step retraction velocities decreased by about a factor of 5 as compared to NaF-free conditions. Importantly, elongated hexagonal etch pits, which are characteristic of (100) surface dissolution, were no longer observed when NaF was present. The alteration of pit shape is more distinct at a higher NaF concentration (50 mM) where triangular etch pits evolved during dissolution. Furthermore, in a fluoride concentration typical for tap water (10 μM), we observed roughening of individual step lines, resulting in the formation of scalloped morphologies. Morphological changes to individual steps across a wide range of fluoride concentrations suggest that the cariostatic capabilities of fluoride ions originate from their strong interactions with molecular steps.

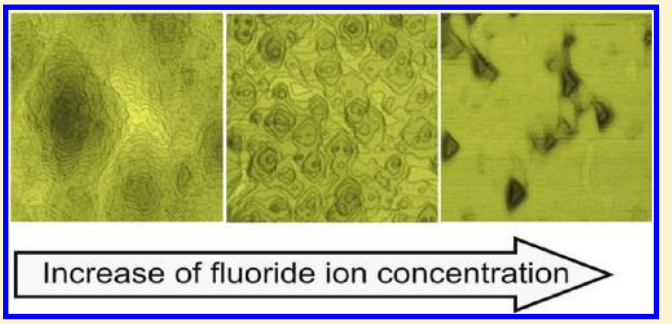

1. INTRODUCTION

Numerous clinical reports have demonstrated that fluoride ion treatment is effective in preventing tooth decay.[1−3] Accordingly, fluoride is used as a common component of toothpastes and mouth rinses, and tap water is fluoridated as a cost-effective method for widespread prevention of dental caries. However, excessive uptake of fluoride causes enamel fluorosis, a condition that causes tooth formation defects, brown stains, and pitting on tooth surfaces.[4−7] There are also controversial links between fluoride and cancers or osteoporosis.[8,9] Although fluoride is critically important to our health, a molecular level understanding of its effects on tooth demineralization and remineralization processes remains elusive[10] due to the complexity of tooth enamel structure, the lack of well-defined model systems, and the technological limitations associated with taking precise measurements on tooth surfaces.

Dental decay is a complex, multistep process initiated by bacteria-induced acid erosion of tooth enamel. The mineral component of enamel is composed mainly of calcium-deficient hydroxyapatite (HAP, $Ca_{10}(PO_4)_6(OH)_2$), crystals with various impurities, mainly carbonate ions.[11,12] The cariostatic effect of fluoride ions originates from their ability to inhibit the initial erosion step. To study this process, bulk solution phase kinetic data, such as transient calcium and phosphate concentrations, have been obtained during apatite dissolution.[13−15] However, bulk solution characterization techniques do not provide information regarding crystal surface phenomena. Therefore, surface-sensitive techniques such as elemental depth profiling using XPS on enamel and synthetic crystals have been performed to provide information on the effects of fluoride treatment on surface chemistry.[16,17] Dissolution inhibition is believed to be accomplished through the incorporation of fluoride ions on HAP surfaces by ion exchange with HAP's hydroxide ions whereby fluoride-substituted apatite surfaces can form, which are several hundred times less soluble than HAP in aqueous solution. In addition, fluoride treatments can create fluoride reservoirs that promote remineralization.[16,18−22] A missing aspect of previous studies on fluoride ion treatment is dynamic, surface structure-dependent information. This information may be critical to our understanding of the role of fluoride ions because reactions occurring at solid/liquid interfaces are significantly influenced by local surface structures such as structural or stoichiometric defects, kinks, and molecular steps as shown in recent microscopic kinetic studies using surface probe microscopy techniques.[23−26] Here, we report on the molecular level mechanism of fluoride ion-mediated inhibition of HAP dissolution by direct observation of atomically well-defined HAP crystal surfaces using atomic force microscopy (AFM). Through real-time observation, we examined the role of the fluoride ions in a concentration dependent manner. On the basis of our

Received: November 3, 2010
Revised: March 16, 2011

dx.doi.org/10.1021/la200325d | *Langmuir* XXXX, XXX, 000–000

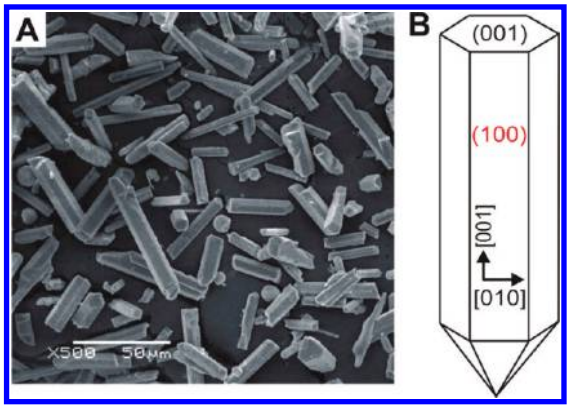

Figure 1. Hydroxyapatite structures. (A) An SEM image of single crystalline HAP. (B) A model of an elongated hexagonal rod-shaped HAP crystal. The specific crystallographic directions and facets are indicated.

observations, we also propose that fluoride ions' cariostatic capabilities in part originate from strong interactions with molecular steps.

2. EXPERIMENTAL SECTION

2.1. Preparation of Single Crystal HAP. We synthesized single crystal HAP using molten salt synthesis.[27] Potassium sulfate was chosen as the molten salt. Amorphous HAP powder (20.0 g) was mixed with potassium sulfate (24.0 g). This mixture was transferred into an alumina crucible and placed inside a furnace. The mixture was heated to 1190 °C over 3 h and cooled naturally by turning off power to the furnace. The mixture inside the furnace was washed three times with DI water to remove potassium sulfate and filtered. The resulting HAP showed an elongated hexagonal rod shape.

2.2. Collection of AFM Images and Data Analysis. All AFM images were obtained in contact mode under pH 6.00 buffer (10 mM, citrate buffer) with different NaF concentrations (spring constant of cantilever: 0.09 N/m) using a commercial AFM (MFP3D, Asylum research, Santa Barbara, CA). To maintain the same NaF concentration during acquisition of AFM images, we flowed buffer containing different NaF concentrations into a fluid cell using a syringe pump (KDS270, KS Scientific, Holliston, MA) with a flow rate of ~10 mL/h. To eliminate the observation of artifacts by the AFM tip due to the high normal forces applied to the HAP surface, we varied the scanning direction, size, angle, and force over the course of image acquisition. Individual step retraction velocities were measured by the end to end distance of the etch pits instead of from a fixed point as a reference to reduce errors that could arise due to thermal drift. By measuring the size of etch pits along the [010] and [001] directions at various time points, we obtained the individual step retraction velocities. From eight different etch pits, which were spatially and temporally unique, we obtained the average step velocities and step densities at various fluoride concentrations. Step density is determined by counting the number of steps per unit length along the [010] or [001] direction.

3. RESULTS AND DISCUSSION

Figure 1A shows an SEM image of HAP obtained by molten salt synthesis.[27] The resulting whiskers have a [001] direction elongated hexagonal rod shape and are mainly covered by six equivalent (100) surfaces (Figure 1B). Powder X-ray diffraction (XRD) patterns of HAP crystals were reported previously (data not shown).[28−30] XRD analysis verified that the crystal phase of our sample is free from α-tricalcium phosphate, which can commonly form during HAP synthesis if the reaction is overheated.

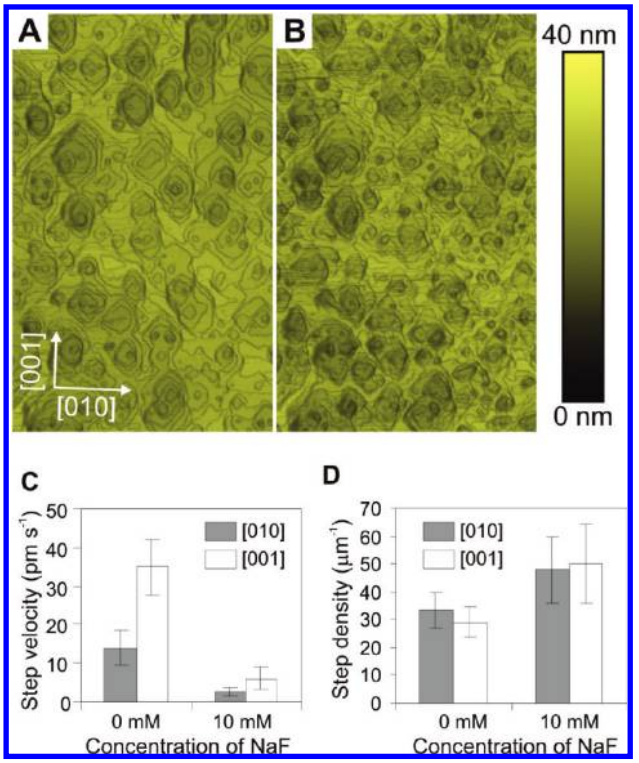

Figure 2. Effect of fluoride ions on HAP dissolution. (A and B) AFM images in pH 6 buffer having 0 M (A) and 10 mM (B) NaF concentration. The shaded bar on the right represents the relative vertical profile. The sizes of the images are 1.0 × 2.0 μm. (C) Dependence of step velocity on the NaF concentration. Two step velocities in pm/s along the [010] and [001] directions are 14 and 35 at 0 M and 2.6 and 6.1 at 10 mM NaF, respectively. (D) Dependence of step density on the NaF concentration across the [010] and [001] directions. Step densities in μm^{-1} along the [010] and [001] directions are 33 and 29 at 0 M and 48 and 50 at 10 mM NaF concentration, respectively.

We observed HAP (100) surfaces under flowing pH 6.00 buffer conditions without and then with 10 mM NaF. Under DI water conditions, the (100) HAP surface exhibited little change over the course of a few hours. With the addition of acidic buffer, the (100) HAP surface began to erode in a surface structure-dependent manner. We initially fixed the total ionic strength at 50 mM using NaCl to minimize ionic strength effects because we previously observed that ionic strength also affects dissolution kinetics.[29] Figure 2A shows an AFM image after 6 h of exposure to acidic buffer without NaF (pH 6.00, 50 mM NaCl). Dissolution proceeded by stochastic formation of elongated hexagonal-shaped etch pits with quantized step heights (~0.82 nm)[28,29] and continued via the retraction of these steps (Figure 2A and movie S1). The step heights corresponded to the interlayer distance between (100) planes. After exposure to NaF-free buffer, we switched the buffer to one containing NaF (pH 6.00, 40 mM NaCl, 10 mM NaF) and observed morphology changes on the (100) HAP surfaces. We measured step velocities in a crystallographic direction-dependent manner by analysis of sequential images that were collected every 260 s. We found that step retraction velocities decreased by about a factor of 5 (Figure 2C) as compared to the NaF-free buffer. Step velocities (pm/s) along

dx.doi.org/10.1021/la200325d |*Langmuir* XXXX, XXX, 000–000

the [010] and [001] directions were 14 and 35 pm/s, respectively, in 0 mM NaF and 2.6 and 6.1 pm/s, respectively, in 10 mM NaF. In addition, we observed that step density on the terrace regions increased in 10 mM NaF conditions (Figure 2D). The step densities along the [010] and [001] directions were 33 and 29 μm^{-1}, respectively, in 0 mM NaF and 48 and 50 μm^{-1}, respectively, in 10 mM NaF. Step density is determined both by the rate of new pit formation and also by the step retraction velocities. New pit formation on a terrace necessarily coincides with the formation of new steps; hence, faster new pit formation increases step density. In contrast, the merging of preexisting steps running in opposite directions results in the annihilation of steps. Therefore, faster step velocities result in decreases in step density. In the case of NaF exposure, the increase of the step density originated from the decrease in step retraction velocities, without a significant change in the rate of new pit formation. Particularly, during the increased duration before step merging in NaF solution, new etch pits evolve on the terrace regions between pre-existing steps. This phenomenon accounts for the increase in the number of small etch pits on the surface when we compare Figure 2A and B. Furthermore, the [001] elongated hexagonal pits are rarely observed in 10 mM fluoride. Instead, pits exhibited a rounder, less regular shape (Figure 2B).

To observe dose-dependent effects of fluoride ions on (100) HAP surface dissolution, we performed additional experiments under higher or lower fluoride concentrations with the same acidic buffer conditions (pH: 6.00). In the case of a higher concentration (50 mM), there is greater inhibition of HAP dissolution, as it takes around 8 h to remove one monolayer from the (100) surface. In addition, the morphological pit shape change is more pronounced. The etch pits evolved into isosceles triangles, which exhibited mirror symmetry across the [010] direction (Figure 3A–C). One important characteristic of the HAP (100) facets is that the (100) surfaces possess a mirror symmetric axis across the [010] direction but not across the [001] direction (Figure 3D). Hence, we can classify the step orientations enclosing the hexagonal pits with four crystallographically distinct steps, which we denoted with a bar, double bar, circle, or square (Figure 3E). Diagonal steps can be divided into two pairs of crystallographically distinct steps ($[011]_+$ and $[0\bar{1}1]_+$ and $[011]_-$ and $[0\bar{1}1]_-$). Similarly, there are two crystallographically nonequivalent steps ($[001]_+$ and $[001]_-$), which are parallel to the [001] direction. Dissolved species can interact differently with crystallographically distinct steps and surfaces, leading to morphology changes during crystal growth and dissolution.[31,32] Particularly, preferential interaction of fluoride ions with the $[001]_-$ steps as compared to the $[001]_+$ steps caused significant retardation of step retraction velocity for the $[001]_-$ steps (Figure 3F). Therefore, the change of relative step retraction velocities in the presence of fluoride ions resulted in evolution of triangular etch pits. It should be noted that the interaction of fluoride ions with HAP steps is currently unique to fluoride ions. Previously, we studied the dependence of the dissolution kinetics of HAP on the concentration of NaCl.[29] We found that the dissolution rate decreased as the concentration of NaCl increased where both step density and step retraction velocities decreased in the presence of NaCl. Although both NaCl and NaF can reduce the dissolution rate of HAP, the change of etch pit shape was not observed in the case of NaCl. Even in 1 M NaCl, the observed elongated hexagonal pit shape is similar in morphology to the NaCl-free conditions (Figure S1). Furthermore, we performed an additional dissolution experiment at a low NaF concentration (10 $\mu M \approx 0.2$ ppm). This concentration is comparable with the concentration of fluoride in tap water. When initially treated with acidic buffer, the (100) HAP surfaces exhibited the elongated hexagonal morphologies (Figure 4A–C). After the infusion 10 μM fluoride, the step lines became roughened and formed a scalloped morphology (Figure 4D–F). This step roughness is a well-known phenomenon attributable to the interaction between molecular steps and step modifiers.[33,34]

Using in situ atomic force microscopy (AFM), the Dove and De Yoreo groups gave detailed descriptions of mineral/water interfaces for individual crystallographic facets of calcite and calcium oxalate surfaces by measuring the dynamic evolution of

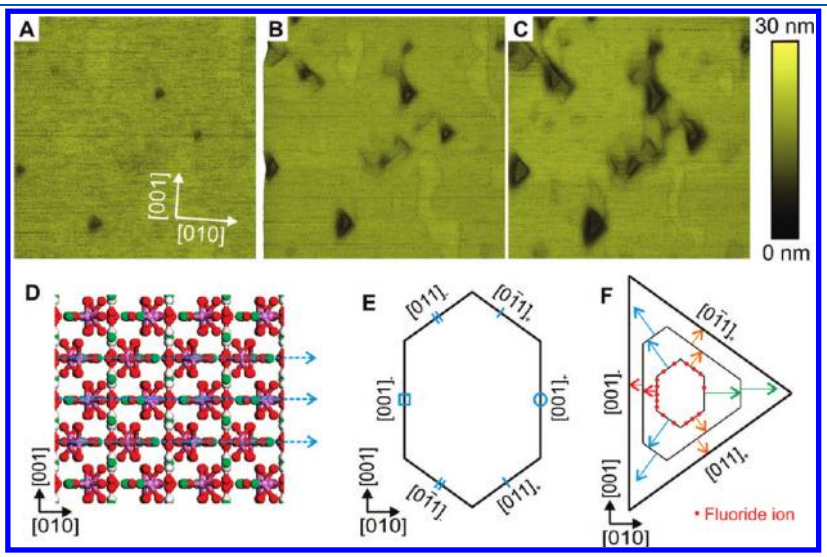

Figure 3. Evolution of a triangular etch pit. (A–C) AFM images at pH = 6.0, 50 mM NaF (size: 1.0 × 1.0 μm, sequential AFM images with time interval 2 h). The right color bar represents relative vertical profile. (D) Surface symmetry of HAP (100) surfaces. Blue lines indicate existence of mirror planes across the [010] direction. (E) Four crystallographically distinct steps enclosing the hexagonal pit (i, $[001]_+$; ii, $[001]_-$; iii, $[011]_+$ or $[0\bar{1}1]_+$; iv, $[011]_-$ or $[0\bar{1}1]_-$). (F) Model of evolution of hexagons to triangle-shaped etch pits. Fluoride ions (red circles) interact differently with four crystallographically distinct steps. Arrows indicate relative step retraction velocities.

dx.doi.org/10.1021/la200325d |*Langmuir* XXXX, XXX, 000–000

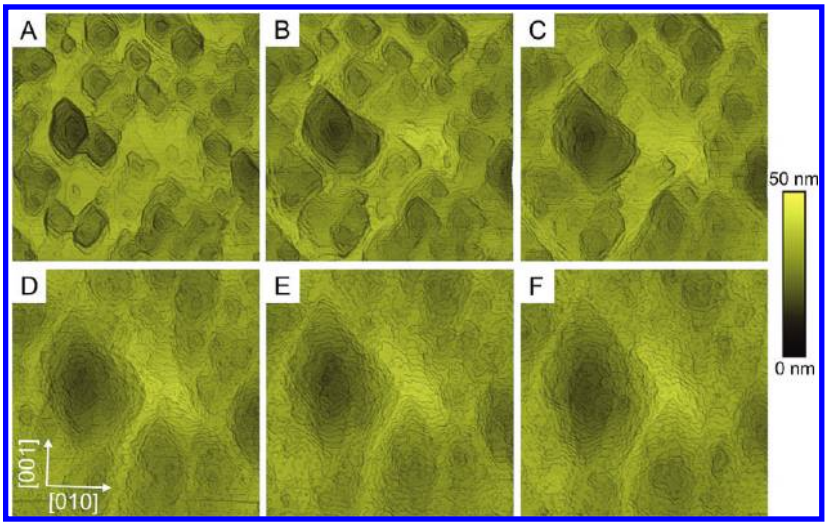

Figure 4. Step roughening under 10 μM NaF concentration (size: 1.4 × 1.4 μm, sequential AFM images with time interval 40 min). Between image frame (C) and (D), the dissolving solution condition is changed from pH = 6.0, no salt concentration, into pH = 6.0, 10 μM NaF concentration. The right color bar represents relative vertical profile.

step heights, step migration velocities, and the frequency of new step formation and disappearance.[34,35] They also reported the effects of a wide range of additives (inorganic salts, amino acids, synthetic peptides, and proteins) on calcite and calcium oxalate mineralization and dissolution and verified their effects on mineralization and demineralization at the molecular level.[26,36,37] These studies demonstrated that the binding of additives to specific molecular steps caused changes in step migration velocities and alterations to the crystals' bulk shapes.[36]

AFM has also been used by several groups to study dental enamel, dentin, bone, and various apatite crystal surfaces.[38−43] These studies have revealed organic−inorganic microstructural interfaces in dental tissues and have measured their micro- and nanoscale properties. However, because of the complexity and inhomogeneity of dental tissues, their molecular structure is generally ill-defined, and studies such as those performed on calcite could not be performed. Various ill-defined synthetic HAP crystals have also been studied under aqueous conditions. To the best of our knowledge, a comprehensive microscopic characterization has not been made due to the lack of a well-defined HAP model system. In this Article, we synthesized well-defined (100) HAP surfaces and investigated the surface morphology evolution under precisely defined fluoride concentration conditions ranging between 10 μM and 50 mM using in situ atomic force microscopy. These fluoride concentration ranges coincide with concentration ranges found in tap water and fluoridated mouth rinses used in dental offices. We observed that the effect of the fluoride on dissolution morphology changes in real time. By comparing dose-dependent etch pit evolution, we observed multiple novel fluoride ion-induced characteristics on (100) HAP surfaces. In the low concentration range (10 μM), we observed scalloped morphologies evolve from the hexagonal-shaped etch pits of the (100) HAP surfaces, which indicates the specific interaction of fluoride with steps. In 10 mM NaF, we could observe that the step retraction velocities of (100) HAP decreased by approximately a factor of 5 as compared to those of fluoride-free condition. In addition, the fluoride significantly altered etch pit shapes such that the initial [001] direction elongated hexagonal etch pits were rarely observed due to the strong inhibition of HAP dissolution. Change of pit shape is more distinct at a higher NaF concentration (50 mM) where triangular pit shapes evolved during the dissolution process.

In summary, we demonstrated that fluoride ions significantly alter etch pit morphology on (100) HAP surfaces by preferential interaction with specific molecular steps using well-defined HAP crystals and in situ AFM techniques. On the basis of our observation of (1) the retardation of step retraction velocity, (2) the concentration dependence of morphological changes on etch pit shape, and (3) scalloped step morphologies, we propose that the cariostatic properties of fluoride on teeth in part originate from strong local interactions with molecular steps. We believe that our molecular level investigation of the (100) HAP surfaces will help us to understand the fundamental mechanism of tooth and bone crystal mineralization and demineralization processes in the future.

■ ASSOCIATED CONTENT

Supporting Information. A dissolution AFM movie (movie S1) and Figure S1. This material is available free of charge via the Internet at http://pubs.acs.org.

■ AUTHOR INFORMATION

Corresponding Author
*E-mail: leesw@berkeley.edu.

■ ACKNOWLEDGMENT

This work was supported by the National Science Foundation Early Career Development Award (DMR-0747713). K.-Y.K. acknowledges support from the National Research Foundation of Korea (NRF-2010-0006157).

■ REFERENCES

(1) Moreno, E. C.; Kresak, M.; Zahradnik, R. T. *Caries Res.* **1977**, *11*, 142.
(2) Leverett, D. H. *Science* **1982**, *217*, 26.

(3) Diesendorf, M. *Nature* **1986**, *322*, 125.
(4) Pendrys, D. G.; Katz, R. V. *Am. J. Epidemiol.* **1989**, *130*, 1199.
(5) Fejerskov, O.; Thylstrup, A.; Larsen, M. J. *Scand. J. Dent. Res.* **1977**, *85*, 510.
(6) Evans, R. W.; Stamm, J. W. *J. Public Health Dent.* **1991**, *51*, 251.
(7) Chen, H.; Czajka-Jakubowska, A.; Spencer, N. J.; Mansfield, J. F.; Robinson, C.; Clarkson, B. H. *J. Dent. Res.* **2006**, *85*, 1042.
(8) Cantor, K. P. *Cancer, Causes Control, Pap. Symp.* **1997**, *8*, 292.
(9) Eastell, R. *N. Engl. J. Med.* **1998**, *338*, 736.
(10) Robinson, C.; Connell, S.; Kirkham, J.; Brookes, S. J.; Shore, R. C.; Smith, A. M. *Caries Res.* **2004**, *38*, 268.
(11) Elliott, J. C. *Structure and Chemistry of the Apatites and Other Calcium Orthophosphates*; Elsevier: Amsterdam, The Netherlands/New York, 1994.
(12) Kay, M. I.; Young, R. A.; Posner, A. S. *Nature* **1964**, *204*, 1050.
(13) Dorozhkin, S. V. *Prog. Cryst. Growth Charact. Mater.* **2002**, *44*, 45.
(14) Tang, R. K.; Nancollas, G. H.; Orme, C. A. *J. Am. Chem. Soc.* **2001**, *123*, 5437.
(15) Guidry, M. W.; Mackenzie, F. T. *Geochim. Cosmochim. Acta* **2003**, *67*, 2949.
(16) MuÃàller, F.; Zeitz, C.; Mantz, H.; Ehses, K.-H.; Soldera, F.; Schmauch, J.; Hannig, M.; HuÃàfner, S.; Jacobs, K. *Langmuir* **2010**, *26*, 18750.
(17) Gerth, H. U. V.; Dammaschke, T.; Schafer, E.; Zuchner, H. *Dent. Mater.* **2007**, *23*, 1521.
(18) Christoffersen, J.; Christoffersen, M. R.; Johansen, T. *J. Cryst. Growth* **1996**, *163*, 304.
(19) Aileen Chin, K. O.; Nancollas, G. H. *Langmuir* **1991**, *7*, 2175.
(20) Ten Cate, J. M.; Duijsters, P. P. E. *Caries Res.* **1983**, *17*, 193.
(21) Cochrane, N. J.; Cai, F.; Huq, N. L.; Burrow, M. F.; Reynolds, E. C. *J. Dent. Res.* **2010**, *89*, 1187.
(22) Jardim, J. J.; Pagot, M. A.; Maltz, M. *J. Dent.* **2008**, *36*, 396.
(23) Schaub, R.; Wahlstrom, E.; Ronnau, A.; Laegsgaard, E.; Stensgaard, I.; Besenbacher, F. *Science* **2003**, *299*, 377.
(24) Kwon, K. Y.; Wong, K. L.; Pawin, G.; Bartels, L.; Stolbov, S.; Rahman, T. S. *Phys. Rev. Lett.* **2005**, 95.
(25) Land, T. A.; DeYoreo, J. J.; Lee, J. D. *Surf. Sci.* **1997**, *384*, 136.
(26) Teng, H. H.; Dove, P. M.; Orme, C. A.; De Yoreo, J. J. *Science* **1998**, *282*, 724.
(27) Tas, A. C. *J. Am. Ceram. Soc.* **2001**, *84*, 295.
(28) Kwon, K. Y.; Wang, E.; Chang, N.; Lee, S. W. *Langmuir* **2009**, *25*, 7205.
(29) Kwon, K. Y.; Wang, E.; Chung, A.; Chang, N.; Lee, S. W. *J. Phys. Chem. C* **2009**, *113*, 3369.
(30) Kwon, K. Y.; Wang, E.; Chung, A.; Chang, N.; Saiz, E.; Choe, U. J.; Koobatian, M.; Lee, S. W. *Langmuir* **2008**, *24*, 11063.
(31) Vavouraki, A. I.; Putnis, C. V.; Putnis, A.; Koutsoukos, P. G. *Cryst. Growth Des.* **2009**, *10*, 60.
(32) Xu, M.; Higgins, S. R. *Geochim. Cosmochim. Acta* **2011**, *75*, 719.
(33) Davis, K. J.; Dove, P. M.; De Yoreo, J. J. *Science* **2000**, *290*, 1134.
(34) De Yoreo, J. J.; Dove, P. M. *Science* **2004**, *306*, 1301.
(35) Qiu, S. R.; Wierzbicki, A.; Salter, E. A.; Zepeda, S.; Orme, C. A.; Hoyer, J. R.; Nancollas, G. H.; Cody, A. M.; De Yoreo, J. J. *J. Am. Chem. Soc.* **2005**, *127*, 9036.
(36) Fu, G.; Qiu, S. R.; Orme, C. A.; Morse, D. E.; De Yoreo, J. J. *Adv. Mater.* **2005**, *17*, 2678.
(37) Orme, C. A.; Noy, A.; Wierzbicki, A.; McBride, M. T.; Grantham, M.; Teng, H. H.; Dove, P. M.; DeYoreo, J. J. *Nature* **2001**, *411*, 775.
(38) Bozec, L.; de Groot, J.; Odlyha, M.; Nicholls, B.; Nesbitt, S.; Flanagan, A.; Horton, M. *Ultramicroscopy* **2005**, *105*, 79.
(39) Kirkham, J.; Brookes, S. J.; Shore, R. C.; Bonass, W. A.; Smith, D. A.; Wallwork, M. L.; Robinson, C. *Connect. Tissue Res.* **1998**, *38*, 91.
(40) Robinson, C.; Connell, S.; Kirkham, J.; Shore, R.; Smith, A. *J. Mater. Chem.* **2004**, *14*, 2242.
(41) Habelitz, S.; Marshall, S. J.; Marshall, G. W.; Balooch, M. *J. Struct. Biol.* **2001**, *135*, 294.
(42) Habelitz, S.; Marshall, S. J.; Marshall, G. W.; Balooch, M. *Arch. Oral Biol.* **2001**, *46*, 173.
(43) Finke, M.; Jandt, K. D.; Parker, D. M. *J. Colloid Interface Sci.* **2000**, *232*, 156.